

Optical satellite imagery detection of internal wave effects from a submerged turbulent outfall in the stratified ocean

R. Norris Keeler

Directed Technologies, Inc., Arlington, Virginia, USA

Valery G. Bondur

“Aerocosmos” Scientific Center, Moscow, Russia

Carl H. Gibson

Scripps Institution of Oceanography, University of California, San Diego, La Jolla, California, USA

Received 9 January 2005; revised 19 May 2005; accepted 20 May 2005; published 28 June 2005.

[1] Sea surface brightness anomalies caused by a municipal wastewater discharge are detected from space in areas much larger than their submerged turbulence source. The mechanism involves a complex interaction between currents, topography, tides, vertical and horizontal mixing, internal waves and stratified turbulence. **Citation:** Keeler, R. N., V. G. Bondur, and C. H. Gibson (2005), Optical satellite imagery detection of internal wave effects from a submerged turbulent outfall in the stratified ocean, *Geophys. Res. Lett.*, 32, L12610, doi:10.1029/2005GL022390.

1. Introduction

[2] In September 2002, 2003 and 2004, major international oceanographic experiments for the monitoring of anthropogenic influences on coastal water areas were carried out in Mamala Bay, Hawaii, employing satellites Ikonos and QuickBird, other spacecraft, 10 ships, several buoy stations and two helicopters. The purpose of the experiments was to study surface manifestations of the Sand Island Honolulu wastewater outfall using optical panchromatic and multispectral images of high spatial resolution along with synoptic microstructure and hydrographic sea truth measurements in the wastewater diffuser vicinity. Mean and micro shear, temperature, conductivity and turbidity sensors were deployed by dropsonde and towed platforms in patterns designed to characterize simultaneous hydrodynamic parameters and stratification in the area of the outfall and receiving waters. Drogues were inserted at the wastewater trapping depth above the diffuser to determine convection paths of the fossil turbulence microstructure patches produced.

2. Observation of Surface Brightness Spectral Anomalies

[3] Figure 1 shows an analysis of a typical space image fragment, obtained on 2 September 2002 by the Ikonos satellite using optical cameras. The satellite cameras took images of an 11 km wide ocean area extending

50 km south-southwest of Oahu. The satellite orbit was sun synchronous at an altitude of 680 km. Image spatial resolution was ~ 1 m in the panchromatic mode and ~ 4 m in the multispectral mode. Figure 1a shows the outfall pipe location ~ 2.5 km distant from shore. Discharged non-salty wastewater (at rates in the range $3\text{--}4$ m³/s) enters Mamala Bay from 283 jets of the 1 km long diffuser section at 68–70 m bottom depths. Horizontal jets mix with dense ocean bottom water to form a buoyant turbulent plume trapped by stable stratification near the pycnocline. The pycnocline depth was 40–50 m. Remnants (fossils) of the turbulence are dispersed by ambient currents. Can the submerged field of advected fossil turbulence patches be detected from satellite images, and at what distances from the diffuser? How is it possible to make this detection?

[4] Obtained space images were processed using a spatial-frequency spectrometry method [Bondur, 2000, 2004]. The method involves 2-D Fourier transformation and specific analysis of the 2-D spatial spectra to allow remote detection of subsurface hydrodynamic processes [Bondur and Grebeniuk, 2001]. The technique is based on registration of slight changes of short (<1 m) surface-wind-driven-waves revealed by anomalous image brightness spectra different from surrounding background areas. Surface manifestations of submerged hydrodynamics can be influenced by the presence of surfactants, but surfactants are reduced to negligible levels by the treatment plant. Ambient surfactants were undetectable. Several spectral anomaly maps found in 2003 and 2004 expeditions extend and support the present 2002 results (C. H. Gibson et al., manuscripts in preparation, 2005a, 2005b) (Available at <http://www-ac.scripps.edu/~ir118>).

[5] Examples of 2-D spatial spectral analysis for two fragments of the 2 September 2002, water-area-image appears in Figure 1a [Bondur and Filatov, 2003]. Figure 1b shows a 2-D spectrum for a background area of ocean surface ~ 5 km west of the diffuser for unaffected surface waves. Figure 1c shows the spectrum for an anomalous spectral region just south of the diffuser, with two EW narrow-band (quasi-coherent) spectral maxima not in Figure 1b that are the detected surface manifestations of the submerged outfall. The wavelength of the EW spectral harmonic ($\nu_0 \sim 0.01075$ m⁻¹) is $\Lambda \sim 93$ m. An enlarged fragment of the anomaly-area-image is given in

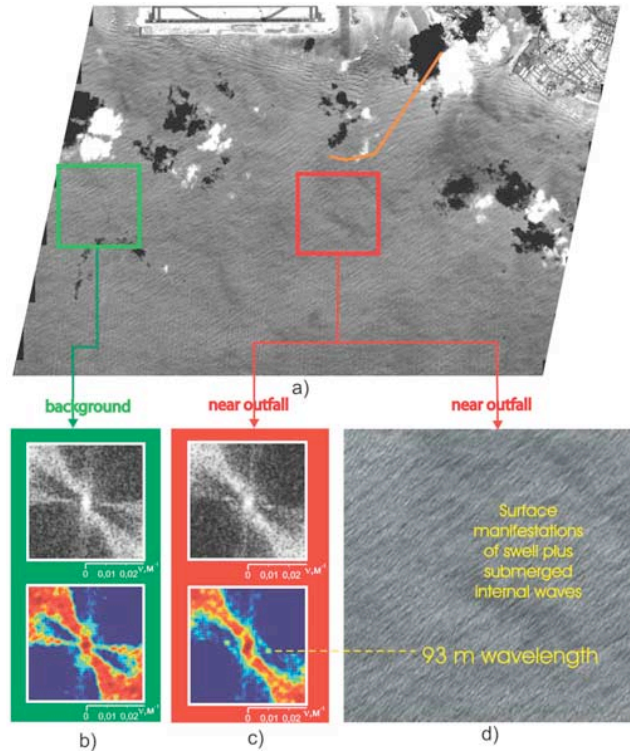


Figure 1. Fragment of Mamala Bay (Honolulu, Hawaii) water area Ikonos image 2002/9/2 with marked location of the (a) outfall pipe, (b) background area, and (c) outfall area. Figure 1d shows area (c) enlarged [Bondur, 2004, 2001].

Figure 1d. Only the NW surface swell can be seen in Figure 1d without processing.

3. Interpretation of Observations

[6] Such spectral anomaly effects of submerged turbulence are detected and described in detail [Bondur, 2000, 2004; Leung and Gibson, 2004; C. H. Gibson et al., manuscripts in preparation, 2005a, 2005b]. The narrow 30–250 m wavelengths $\Lambda \approx L_{R_0}$ reflect near-vertically-propagating fossil-turbulence-waves (FTWs) from bottom turbulence events with fixed ε_0 and $N = [-(g/\rho)\partial\rho/\partial z]^{1/2}$, and large Ozmidov scales at beginning of fossilization $L_{R_0} \equiv (\varepsilon_0/N^3)^{1/2}$. Information about these soliton packets is beamed to the surface by reactivated outfall fossil turbulence patches (zombies), as discussed in the following section. It is usually assumed that internal wave surface manifestations reflect surface convergences smoothing short surface wind-waves by advected surfactants increasing surface tension, but this assumption is oversimplified from the present observations.

[7] To determine the extent of the outfall surface anomalies, 2-D brightness spectra of various fragments of the satellite image were analyzed. First, $2 \times 2 \text{ km}^2$ fragments (Figures 1b, 1c, and 1d) were examined. Then, $1 \times 1 \text{ km}^2$ regions were analyzed for more accurate localization of the whole anomalous area, its form, and its surface-wave intensity variation [Bondur, 2004]. The results are shown in Figure 2a, where two regions, or lobes, of anomalies were found; one extending more than $12 \times 5 \text{ km}^2$ to the SW, and

a second $6 \times 2 \text{ km}^2$ to the SE of the diffuser. During sea truth experiments it was observed that drogues released at the wastewater trapping depth over the diffuser traveled occasionally and unpredictably in these two directions [Leung and Gibson, 2004; C. H. Gibson et al., manuscripts in preparation, 2005a, 2005b]. Acoustic-Doppler-Profiler (ADP) measurements gave 3-D progressive-vector diagrams from currents near the diffuser that deepened to the SW (Figure 2b) on the test day, consistent with the extensive SW area of the surface anomalies. Currents at the outfall reflect a combination of EW tidal flows, NW surface onshore drift, and S-SE-SW offshore flows induced by island fresh water runoffs. Larger and smaller single and double lobe anomaly patterns like Figure 2a have now been observed in many Ikonos and QuickBird space images for other days of the complex experiments (C. H. Gibson et al., manuscripts in preparation, 2005a, 2005b).

4. Fluid Mechanical Model

[8] The existence of space-detectable submerged stratified turbulence manifestations at such extraordinary distances from the outfall diffuser came as a complete surprise. Somehow information about submerged turbulence in the near vicinity of the diffuser pipe propagates to large distances from the source and reaches the surface. Detailed analysis of the physical mechanisms responsible for such phenomena is given by Bondur [2000, 2004], Leung and Gibson [2004], and C. H. Gibson et al. (manuscripts in

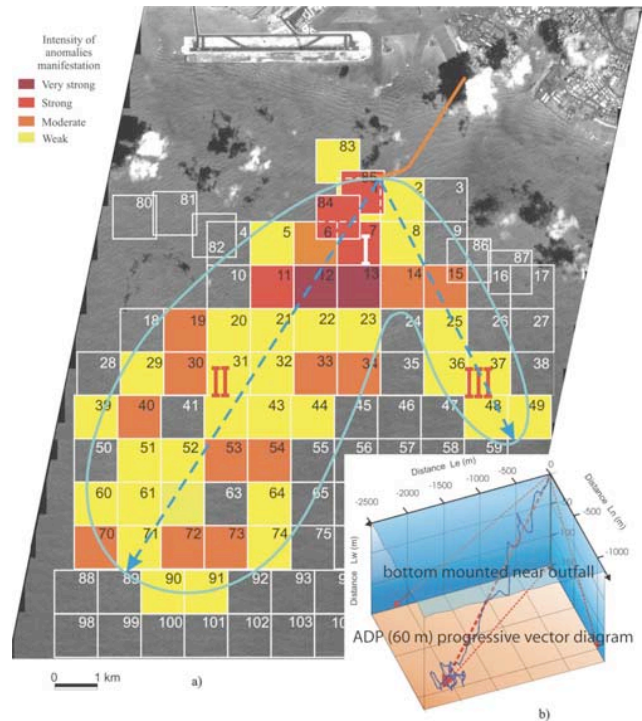


Figure 2. Spatial distribution of anomalous spectral brightness caused by submerged outfall turbulence in 1 km areas of the (a) space image and (b) progressive-vector 60 m flow near the diffuser from the bottom mounted ADP [Bondur and Filatov, 2003].

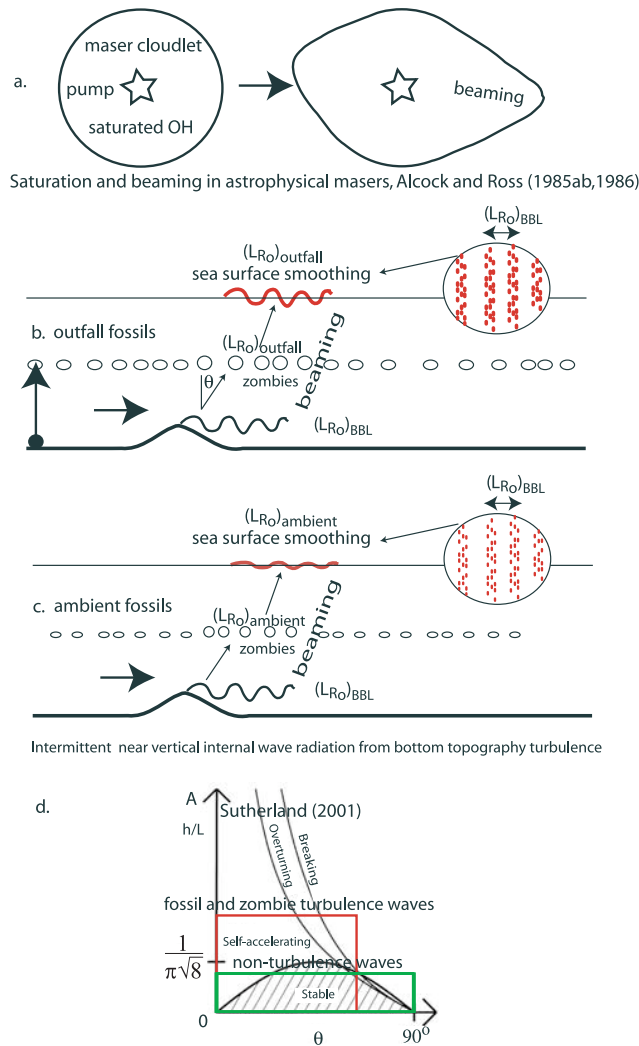


Figure 3. Beamed zombie turbulence maser action (BZTMA) mixing chimney model (C. H. Gibson et al., manuscript in preparation, 2005a).

preparation, 2005a, 2005b). Further experiments are planned and various models are under test.

[9] Turbulence is defined as an eddy-like state of fluid motion where the inertial-vortex forces ($\vec{v} \times \vec{\omega}$) are larger than any of the other forces that tend to damp the turbulence out. Turbulence is rotational and always cascades from small scales to large. Fossil turbulence is a perturbation in any hydrophysical field ($\rho, T, S, \vec{\omega}$) caused by turbulence that persists after the fluid is no longer turbulent at the scale of the perturbation [Gibson, 1986, 1999]. Scrambled density regions are termed fossil-density-turbulence, for example.

[10] Fossil-density-turbulence patches are advected away from the diffuser by deepening off-shore currents at the trapping depth, as shown by ADP data (Figure 2b) and by parachute drogues set near the trapping depth. Tilting of strong density gradients bounding ~ 8 m fossil-density-turbulence outfall patches produces vorticity (and zombie turbulence) from baroclinic torques at rates $(\nabla \rho \times \nabla p)/\rho^2$, Figure 3. This extracts energy from (30–250 m) ambient internal waves in detectable patterns that reflect the tilt fields, directions, and narrow frequency bands of the

larger waves. Fossil-vorticity-turbulence motions of fossil-density-turbulence microstructure patches then couple to the overlying stratified water layers and radiate secondary, near-vertical ($\sim 45^\circ$), fossil-turbulence and zombie-turbulence internal-waves (FTWs, ZTWs) that carry information to the sea surface about wavelengths and directions (the tilt patterns) of the soliton internal waves that reactivate the outfall fossils.

[11] The smaller scale secondary waves (ZTWs) break when they encounter the surface solar-heated wind-mixed layer. The resulting turbulence and its fossils locally smooth the sea by interfering with short capillary and gravity-capillary surface waves. The anomalous ocean surface brightness patterns of otherwise invisible submerged fossils and soliton internal waves may then be detected remotely as shown in Figures 1 and 2. Turbulence in contact with stably stratified fluids [Sutherland and Linden, 1998; Diamessis et al., 2005] produces near-vertically-propagating ($\sim 45^\circ$) internal waves (termed Linden-Sutherland waves) at L_{R_0} scales taken to be equivalent to FTWs and ZTWs, as shown in Figures 3b, 3c, and 3d (C. H. Gibson et al., manuscript in preparation, 2005a). Amplified and beamed vertically by previous ZTW trails of fossil-turbulence-patches, FTWs from bottom topography events can form near-vertical beams, or chimneys (C. H. Gibson et al., manuscript in preparation, 2005b), analogous to the beamed radiation (Figure 3a) of astrophysical masers [Alcock and Ross, 1985a, 1985b, 1986].

5. Microstructure Measurements

[12] Surface ϵ values measured ~ 100 m NW of the diffuser (region 83 of Figure 2a) were $\sim 10^2$ larger than simultaneous ambient values 400 m E and 600 m W (C. H. Gibson, manuscript in preparation, 2005a). Profiles and photographs show vertical turbulent mixing did not directly transmit either wastewater or information about the submerged outfall turbulence detected in region 83. In 2002, hydrodynamic states of ~ 1400 microstructure patches were

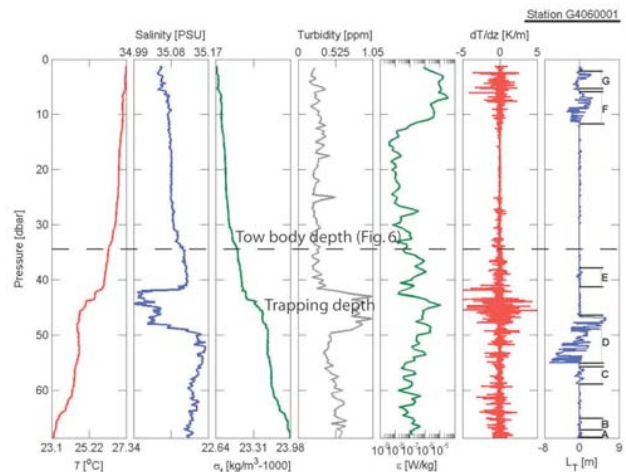


Figure 4. Vertical profiles of temperature T, salinity S, density σ , turbidity, viscous dissipation rate ϵ , temperature gradients, and Thorpe density displacement scales L_T 50 m NW of the end of the diffuser, on 2 September 2002 [Leung and Gibson, 2004].

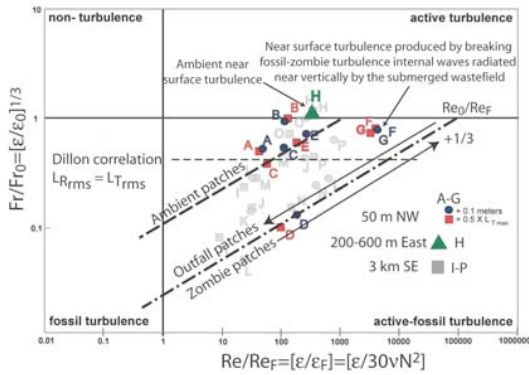


Figure 5. Hydrodynamic phase diagram for microstructure patches, emphasizing points A–G near the end of the diffuser (Figure 4) [Leung and Gibson, 2004].

determined by hydrodynamic phase diagrams. Many of the 200 active turbulent patches found were small (~ 1 m) and located above and below fossilized larger patches, suggesting vertical radiation of near-critical fossil-turbulence-waves (FTWs) by damped turbulence (fossil-vorticity-turbulence) patches that initially bob as non-propagating saturated-internal-waves at the local stratification frequency N . These are created in a brief time $t \leq N^{-1}$ as active turbulence fossilizes. From a much larger sample in 2003, only three patches with $Re_0/Re_F \approx 10^4$ were detected near the outfall in their fully turbulent state, showing the brevity and intermittency of these dominant turbulent events. Ambient patches have $Re_0/Re_F \leq 10^3$.

[13] Figure 4 shows vertical profiles of microstructure variables measured ~ 50 m NW of the end of the diffuser pipe, with the trapped wastewater signature (low S , high turbidity) at a depth of 42–50 m [Leung and Gibson, 2004]. Because the waste field was completely trapped by the stratification, we are forced to conclude that the strong near-surface turbulence observed in patches F and G reflects near surface FTW and ZTW breaking. Patch E is a deep active turbulence patch also caused by upward FTW radiation. Further evidence of FTW breaking above the waste field is given by the strong temperature gradients of fossil-temperature-turbulence just above patch D (Figure 4).

[14] The hydrodynamic state of microstructure patches is determined using hydrodynamic phase diagrams [Gibson, 1986] as shown in Figure 5 for the patches of Figure 4. The viscous dissipation rate ε is measured for the studied patches by shear probes on the microstructure profiler. The stratification frequency N is computed from the ambient density gradient. The y-axis of Figure 5 $Fr/Fr_0 = (\varepsilon/\varepsilon_0)^{1/3}$ is the ratio between the Froude number of the patch detected with dissipation rate ε and a patch with the same size L and stratification N values at its beginning of fossilization with dissipation rate ε_0 , where $\varepsilon_0 \approx 3L_T^2 \max N^3$. The x-axis of Figure 5 is the normalized patch Reynolds number $Re/Re_F = \varepsilon/\varepsilon_F$, where $\varepsilon_F = 30\nu N^2$ and ν is the kinematic viscosity. Fossil decay and zombie patch growth should occur approximately along loci of slope $+1/3$, as shown. The zombie turbulence patch D (with false $Re_0/Re_F \approx 10^5$) is classified as active-fossil-turbulence in Figure 5, meaning that the energy of the largest turbulence scales has been converted to fossil-vorticity-turbulence

internal-wave motions with frequency $\sim N$, and the smallest scales are still overturning active-turbulence. The dashed line in Figure 5 shows the Dillon correlation $L_{R_{rms}} = L_{T_{rms}}$, which has been interpreted as showing microstructure patches are turbulence in equilibrium with the ambient stratification and that fossil turbulence does not exist. However, $L_{T_{rms}}$ values for patches in the active-fossil quadrant preserve information about ε_0 because $L_{T_{rms}} \sim L_{T_{max}} \sim L_{R_0}$. Figure 5 shows no evidence of a correlation between L_R and L_T for individual patches, or any failure of the fossil turbulence paradigm.

[15] Figure 6 shows averaged regions of temperature gradient variance measured from the towed microstructure instrument package above the trapping depth (Figure 4) to detect anomalous mixing by fossil-zombie-turbulence-waves propagating to the sea surface. The mixing pattern of Figure 6 matches the SW-SE surface-brightness pattern in Figure 2a. A drogue track shows SE wastewater advection in the direction of the SE lobe. Internal waves radiate from a turbulent wake after fossilization at $\sim 45^\circ$ with wavelength $\Lambda \approx L_{R_0}$ [Diamessis et al., 2005, Figure 6].

6. Conclusions

[16] Satellite optical imagery from 680 km is able to detect surface manifestations in ~ 70 km² areas for submerged stratified turbulence caused by a buoyant municipal outfall wastewater field injected at the bottom with an initial trapped horizontal surface area less than 0.1 km². Observed phenomena are related to the wastewater discharge from Sand Island (Mamala Bay, Hawaii) originating at an offshore distance of ~ 2.5 km from the diffuser 70 m below the ocean surface, and confined by stratification to below 40 m. Narrow-frequency-band surface brightness spectral anomalies were remotely detected >12 km from their origin.

[17] The narrow-spatial-frequency character of the surface-brightness spectral anomalies of Figures 1 and 2 and other studies (C. H. Gibson et al., manuscripts in preparation, 2005a, 2005b) in the wavelength range 30–250 meters supports the conjecture that these reflect large-amplitude FTWs radiated intermittently and near-vertically from bottom topography turbulence events. Energy and anomaly information (Λ , θ) from these soliton-waves is beamed to the surface by smaller fossil-zombie-turbulence-patches from the Sand Island outfall according to the BZTMA

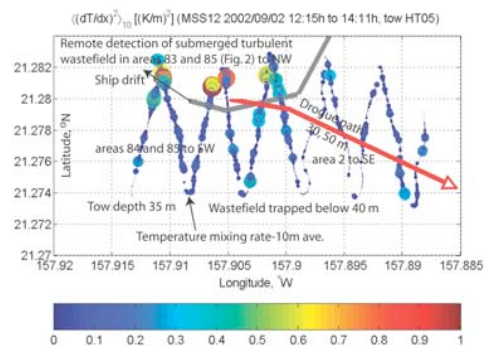


Figure 6. Circle sizes and colors indicate 10-m averages of temperature gradient variance $\sigma(T_x) = \langle (dT/dx)^2 \rangle$ along a towpath above the 40–50 trapping depth, at ~ 35 m.

mechanism of Figures 3b, 3c, and 3d. From hydrodynamic phase diagrams (HPDs, Figure 5) we find outfall fossils persist with $Re_0/Re_F \approx 25,000$, versus ambient fossils with $Re_0/Re_F \approx 10^3$. We associate fossil-zombie-turbulence-waves with large-amplitude Linden-Sutherland waves (Figure 3d) studied by laboratory experiments and by non-linear computer modeling [Sutherland and Linden, 1998; Diamessis et al., 2005]. Field evidence from 2002 is given in the vertical and horizontal microstructure measurements and analysis of Figures 4, 5, and 6. Zombie outfall turbulence patches are indicated from HPDs with $Re_0/Re_F \approx 10^5$ for times inferred from drogue advection speeds and distances $t > 300N^{-1}$. Deep profiles in 2004 show fossils of bottom boundary layer events with $Re_0/Re_F \approx 10^6$ (C. H. Gibson et al., manuscript in preparation, 2005b). Further data analysis and field measurements, as well as laboratory experiments, computer modeling, and theoretical studies, are required to test our interpretations of these extremely complex processes.

References

- Alcock, C., and R. R. Ross (1985a), Saturation and beaming in astrophysical masers, *Astrophys. J.*, *299*, 433–454.
- Alcock, C., and R. R. Ross (1985b), Saturation and beaming in astrophysical masers. II. The fully saturated limit, *Astrophys. J.*, *299*, 763–768.
- Alcock, C., and R. R. Ross (1986), Saturation and beaming in astrophysical masers. III. Asymmetrically pumped masers, *Astrophys. J.*, *306*, 649–654.
- Bondur, V. G. (2000), *Studies in the Areas of Oceanology, Atmospheric Physics, Geography, Ecology, Ocean-Related Problems, and Geocryology*, edited by Y. A. Israel, 254 pp., Russ. Acad. of Sci., Moscow, Russia.
- Bondur, V. G. (2004), *New Ideas in Oceanology*, vol. 1, *Physics, Chemistry, Biology*, edited by M. E. Vinogradov and S. S. Lappo, pp. 55–117, Nauka, Moscow.
- Bondur, V. G., and N. N. Filatov (2003), Study of physical processes in coastal zone for detecting anthropogenic impact by means of remote sensing, *Proceedings of the 7th Workshop on Physical Processes in Natural Waters*, edited by A. Terzhevik, pp. 98–103, Inst. of Water Probl. of the N., Karelian Sci. Cent., Russ. Acad. of Sci., Petrozavodsk, Russia.
- Bondur, V. G., and Y. V. Grebeniuk (2001), Remote indication of anthropogenic influences on marine environment caused by deep outfalls (in Russian), *Issled. Zemli Kosmosa*, *6*, 49–67.
- Diamessis, P. J., J. A. Domaradzki, and J. Hesthaven (2005), A spectral multidomain penalty method model for the simulation of high Reynolds number localized incompressible stratified turbulence, *J. Comput. Phys.*, *202*, 298–322.
- Gibson, C. H. (1986), Internal waves, fossil turbulence, and composite ocean microstructure spectra, *J. Fluid Mech.*, *168*, 89–117.
- Gibson, C. H. (1999), Fossil turbulence revisited, *J. Mar. Syst.*, *21*, 147–167. (Available at <http://xxx.lanl.gov/abs/astro-ph/9904237>.)
- Leung, P. T., and C. H. Gibson (2004), Turbulence and fossil turbulence in oceans and lakes, *Chin. J. Oceanol. Limnol.*, *22*, 1–23. (Available at <http://xxx.lanl.gov/abs/astro-ph/0310101>)
- Sutherland, B. R. (2001), Finite-amplitude internal wavepacket dispersion and breaking, *J. Fluid Mech.*, *429*, 343–380.
- Sutherland, B. R., and P. F. Linden (1998), Internal wave generation by flow over a thin barrier, *J. Fluid Mech.*, *377*, 223–252.
- V. G. Bondur, “Aerocosmos” Scientific Center, 105064 Moscow, Russia.
- C. H. Gibson, Scripps Institution of Oceanography, UCSD, MAE/SIO Mail Code 0411, 9500 Gilman Drive, La Jolla, CA 92093–0411, USA. (cgibson@ucsd.edu)
- R. N. Keeler, Directed Technologies, Inc., 3601 Wilson Blvd. Suite 650, Arlington, VA 22201, USA.